AW-OSEM PARAMETER OPTIMIZATION FOR SELECTED EVENTS RELATED TO THE BREATH-HOLD CT POSITION IN RESPIRATORY-GATED PET ACQUISITIONS.

J. Daouk, L. Fin, P. Bailly, M.-E. Meyer

Nuclear Medicine Department, Amiens University Hospital, F-80054 Amiens, France

ABSTRACT

We present a novel CT-based method for minimizing the influence of respiratory motion in positron emission tomography (PET) images. The method relies on selection of events (i.e. detected coincidences) corresponding to the respiratory state in breath-hold X-ray computed tomography (CT) from respiratory-gated List Mode (LM) acquisitions. The low counting statistics in this method prompted an assessment of the tradeoff between the bias in standard imaging with motion and the increased variance associated with only using counts from a single phase of the respiratory cycle.
The influence of AW-OSEM parameters (the number of iterations and the 3D Gaussian postfilter settings) was also optimized to suit the low counting statistics.
Our results show that the parameter-optimized CT-based method reduces bias to 37.3%, compared with 70.7% for standard images with motion.

Index Terms — positron emission tomography; X-ray tomography; respiratory motion compensation; image reconstruction optimization.

1. INTRODUCTION

The principle of iterative data reconstruction in positron emission tomography (PET) is based on a hypothesis whereby the structures located in the object field are immobile. In fact, the algorithms based on maximum likelihoods (such as the Ordered Subsets Expectation Maximization (OSEM) algorithm), now used widely in routine clinical practice, incorporate a statistical model of photon emission from a static radioactive element [1]. Hence, this hypothesis is inherently flawed for acquisitions performed on mobile organs - notably those in the thoracic or abdominal regions undergoing respiratory motion.
In routine clinical practice and because acquisitions typically last several minutes, certain anatomical structures are subject to physiological motion, leading to a spread in their activity projection [2]. This spreading results in poor evaluation of the uptake intensity of these mobile organs in the final, reconstructed images. Bias is defined as the relative difference between the real activity and the corresponding value given by the reconstruction algorithm. It has been shown that in the absence of motion, bias depends on target size and reconstruction parameters (around 70% for 1 cm diameter spheres with a 6-mm, three-dimensional Gaussian filter) [3]. This bias is likely to be altered in the presence of any motion. Solving the spreading problem is thus of significant interest for calculation of standardized uptake value (SUV) - a process which requires the most accurate possible voxel value.
Smearing effects can be reduced by using List Mode (LM) respiratory-gated PET acquisition (RG-PET). Generally, RG-PET processing divides each respiratory cycle into several time intervals [4]. The disadvantage of these methods is that several volumes are generated for only one quasi-instantaneous CT scan. Thus, the attenuation correction can be erroneous and lead to bias in the quantification, especially for moving lesions at the edge of anatomical regions with different densities (e.g. lower lung and liver dome, etc.).
We previously developed a RG-PET processing method which generates a single PET volume (CT-based) related to a breath-hold CT acquisition (BH-CT), guaranteeing a good match between PET and CT volumes [5]. The goal of the present work was to study the effect of this method on the bias in PET images and to optimize reconstruction parameters when only a part of the counting statistics is used.

2. MATERIALS AND METHODS

2.1. Data acquisition

The study was performed using a phantom centered in the useful field of view (UFOV). It consisted of a rubber balloon filled with an 18F-fluorodeoxyglucose (18F-FDG) solution (62.5 kBq/ml) containing 0.5% of iodized contrast agent (1.5 mg/ml), placed in the body phantom of the NEMA IEC Body Phantom Set™ (Data Spectrum Co., Hillsborough NC, USA). A sphere (0.5 ml, inner diameter = 9.89 mm) (Data Spectrum Co., Hillsborough NC, USA) filled with an 250 kBq/ml 18F-FDG solution moved parallel to the table axis. The sphere was tangential to the balloon in the expiration state and, when moving, pushed on the balloon's mid-section (see Fig. 1). The motion was set to 15 cycles per minute, with an amplitude of 20 mm. Scattering layers were placed above and below the phantom. The 18F-

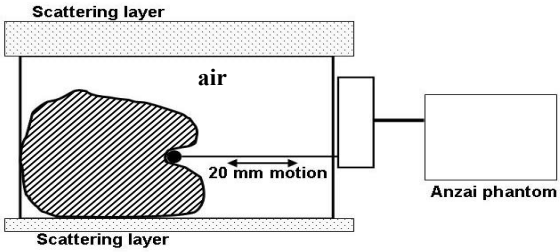

Fig. 1. Diagram of the experimental setup. The Anzai phantom features rectilinear motion of 20 mm

FDG sphere-to-background contrast of 4:1 was checked with a gamma counter.

All acquisitions were performed on a Biograph™ 6 (Siemens Medical Solutions, Erlangen, Germany) in 3D mode. Random events were collected in a delayed window. Respiratory gating was achieved with the Anzai AZ733V system (Anzai Medical Co. Ltd., Tokyo, Japan).

Ten separate 10-minute LM acquisitions were performed with simultaneous respiratory signal recording. The phantom was not moved until the end of the whole study. Lastly, a 3-minute reference image (REF) acquisition was performed in the same table position, with the phantom in the expiratory state but in the absence of motion.

Two CT scans were also performed: one in a 'free breathing' state ("CT-std": 110 kV, 150 mA, with a pitch of 1:1, collimation 6 x 2.0 mm, gantry rotation time 0.6 s) and the other in a shallow 'end expiration' state ("BH-CT": 110 kV, 83 mA, with a pitch of 1:2, collimation 6 x 2.0 mm, gantry rotation time 0.6 s) with the sphere away from the balloon in order to generate attenuation correction maps. In a previous study, we showed that the BH-CT parameters only deliver a very small additional effective dose to patients ($D_{Eff} \approx 0.68$mSv) [5].

2.2. Data reconstruction

All data were reconstructed in volumes of 168x168x81 voxels (i.e. voxel size of 4.06x4.06x2 mm^3) with FORE [6] + AW-OSEM. Random events were subtracted from prompt events. Attenuation correction (AC) coefficients at 511 keV were calculated from a CT acquisition [7]. Scatter correction was performed according to Watson's method [8].

For each LM acquisition, an Ungated volume (corresponding to the whole 10-minute acquisition) was reconstructed using routine clinical parameters: 4 iterations (it) and 8 ordered subsets (os) with an isotropic Gaussian 3D-post-filter (GPF) with FWHM = 5 mm. AC was based on CT-std.

The REF volume was reconstructed using 4 it, 8 os and a GPF with a FWHM of 2 mm.

BH-CT acquisition was performed after RG-PET. The position of the breath-hold was clearly visible on the respiratory curve and allowed manual placing of an event selection range (ESR) around this position (see Fig. 2). The portions of the respiratory curve which fell within this ESR defined the portions of the LM for binning into a CT-based sinogram. In the present study, the ESR was set to 10 % of the respiratory signal's overall amplitude. Each CT-based sinogram was reconstructed with 1, 2, 4, 6, and 8 iterations, 8 subsets and an isotropic GPF with FWHM = 2, 3, 4 and 5 mm. For the CT-based and REF volumes, AC was based on the BH-CT scan.

Ultimately, 1 REF volume, 10 Ungated volumes and 200 CT-based volumes (i.e. 10 acquisitions x 5 different iteration numbers x 4 different GPF widths) were generated.

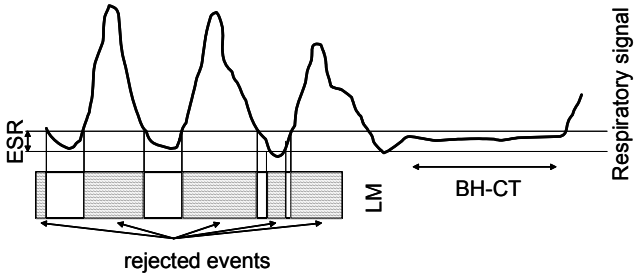

Fig. 2. The CT-based methodology: respiratory signal during breath-hold CT (BH-CT) indicates the tissue position.

2.3. Data analysis

Bias-variance plots were used to assess not only the tradeoffs between the bias of Ungated imaging with motion and the increased variance associated with only using counts from a single phase of the respiratory cycle but also the optimal reconstruction parameters for a given set of counting statistics.

PET volumes of interest (VOIs) were segmented on the sphere according to Nestle's algorithm [9] (one for the Ungated volume and one for all the CT-based volumes). For each reconstructed volume, we considered bias and variance [10] in the two VOIs over the 10 acquisitions, according to the following equation:

$$Bias = \left(\frac{1}{nb\_voxels} \sum_{i=1}^{nb\_voxels} \left| \overline{v_i} - v^{true} \right| \right) \times \frac{100}{v^{true}} \quad (1)$$

where nb_voxels is the number of voxels in the considered VOI, v^{true} is the measured activity concentration inside the sphere and $\overline{v_i}$ is the average of the i-th voxel value over the 10 acquisitions, computed as follows:

$$\overline{v_i} = \frac{1}{10} \sum_{j=1}^{10} v_i^j \quad (2)$$

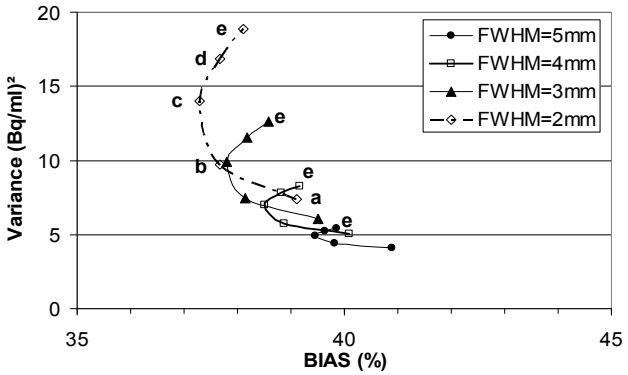

Fig. 3. The bias-variance plots for each Gaussian post-filter and for (a) 1 it, (b) 2 it, (c) 4 it, (d) 6 it and (e) 8 it (8 os in all cases).

where j is the index of the acquisition and v_i^j is the i-th voxel value of the j-th acquisition.
The variance of a sequence of volumes is defined as:

$$Variance = \frac{1}{nb\_voxels \times 10} \sum_{i=1}^{nb\_voxels} \sum_{j=1}^{10} (v_i^j - \overline{v_i})^2 \quad (3)$$

3. RESULTS

3.1. Counting statistics

The average single rate for phantom acquisitions was 8,117 ± 1,428 kcps. This activity in the UFOV is coherent with the activity found in a PET acquisition of an UFOV covering the liver dome (average single rate = 7,805 ± 884 kcps, calculated with 10 patients).

3.2. The bias-variance tradeoff

Segmented VOIs were 3.89 ml (118 voxels) for Ungated volume and 0.53 ml (16 voxels) for all CT-based volumes.
The results of our bias and variance calculations are shown in Figure 3. Ungated volumes gave bias and variance values of 70.7% and 0.7 (Bq/ml)², respectively (not shown on the plot for more clarity). Depending on the exact reconstruction parameters used, CT-based volumes displayed bias values from 40.9% down to 37.3%.
SUV_{MAX} are presented in Table 1 for Ungated, CT-based (4 it, 8 os, FWHM = 2 mm) and REF volumes. Figure 4 presents cross-sectional images for the same volumes. In the Ungated image (see Fig. 4.a), the uptake is smeared along the 20mm-course of the sphere, whereas the sphere's shape is better defined and has enhanced contrast in both CT-based and REF images (see Fig. 4.b and 4.c).

4. DISCUSSION

The aim of this work was to study the bias obtained for CT-based images as a function of the AW-OSEM reconstruction algorithm parameters.

Table 1. SUV_{MAX} measured for the balloon and the sphere for three different volumes.

	Balloon	Sphere
Ungated 4it, 8 os, FWHM = 5 mm	0.9	0.9
CT-based 4it, 8 os, FWHM = 2 mm	0.9	2.4
REF 4it, 8 os, FWHM = 2 mm	0.9	2.6

The ESR of 10% is a satisfactory tradeoff between counting statistics and motion reduction and corresponds to a 135s-acquisition time.
Compared with the Ungated method, the CT-based method reduces bias (from 70% down to 37-41%). This reduction results from (i) motion elimination due to event selection and (ii) more accurate attenuation correction.
The results in Figure 3 show that both the number of iterations and the FWHM of the GPF have an impact on quantification in PET images. For a given GPF, the reconstruction algorithm converges to an optimal solution and then diverges. Indeed, the first iterations bring low frequencies into the image, whereas the last iterations bring high frequencies (that is to say, boundaries and noise). To minimize bias in a 168x168 matrix, the optimal iteration is 4 it/8 os for a 10 mm diameter object, whatever the GPF setting.
The calculated variance serves as an estimate of the numerical stability of AW-OSEM with different parameters. Indeed, reconstructing PET data remains a critical issue, since it requires the resolution of an ill-posed, inverse problem in which a few noise in the acquired data may produce significant noise in the final image [11]. There are various ways of dealing with this issue: (i) stopping rules, (ii) true regularization (via priors or penalization) and (iii) noise-reduction methods (e.g. postfiltering). The latter solution is imposed by the Biograph system. The GPF with a FWHM = 2 mm yields the lowest bias (Low_Bias_2mm = 37.3%) and the highest variance. This can be explained by the fact that this filter least alters spatial resolution but also leaves noise. In contrast, the GPF with a FWHM = 5 mm smoothes the images more - reducing noise but altering the spatial resolution more (Low_Bias_5mm = 39.5%). The GPF with a FWHM = 2 mm is the best choice, especially since the bias is reduced by 2% with an increase of the variance of only 1.4 x 10^{-8}%.

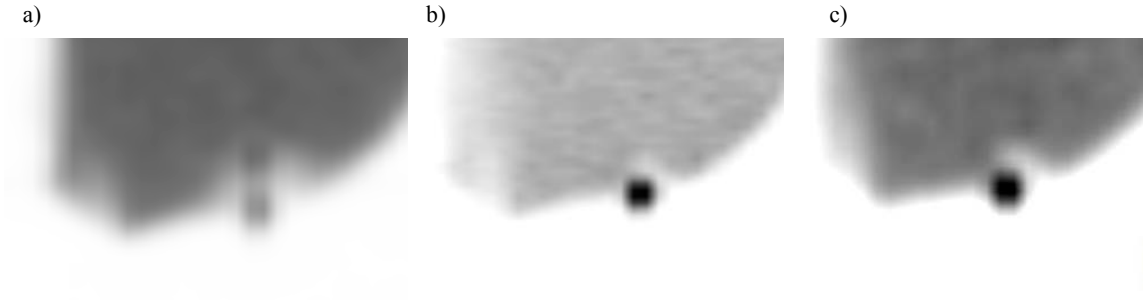

Fig. 4. Sagittal cross-section passing through the sphere for the (a) Ungated volume, (b) CT-based (4it, 8 os, FWHM = 2 mm) volume, (c) REF volume.

The sphere and the balloon were chosen to mimic tumor behavior in the vicinity of the liver dome, which is a known site for respiratory artifacts [2]. The density in the balloon obtained with 0.5% iodized contrast agent corresponds to the Hounsfield units typical seen in the liver.

Although the average single rate corresponds to values typically measured in patient acquisitions on the liver dome, the standard deviation is higher for the phantom because of the radioactive decay between each acquisition over the whole experiment. The random rate also corresponds to typical clinical values. The parameters optimized for this study (i.e. optimized for the noise introduced by random subtraction) remain optimized for clinical use.

When reconstructed with optimized parameters, SUV_{MAX} for the CT-based method tends towards SUV_{MAX} measured in REF images. The tiny difference is due to the lower counting statistics and the residual motion, within the 10% ESR, for the CT-based method.

5. CONCLUSION

Even though part of the counting statistics is discarded, this study establishes that our CT-based method increases the accuracy of contrast, quantification and PET-CT registration when compared with standard Ungated volume and is not accompanied by a major increase in the variance.

Moreover, we have determined that the optimal OSEM parameters for these low counting statistics are 4 iterations, 8 ordered subsets and a GPF of FWHM = 2mm.

6. ACKNOWLEDGMENTS

This work was funded by the Canceropôle Nord Ouest France.

7. REFERENCES

[1] C. Comtat, P. E. Kinahan, M. Defrise *et al.*, "Fast reconstruction of 3D PET data with accurate statistical modeling," *IEEE Transactions on Nuclear Science,* vol. 45, no. 3, pp. 1083-1089, Jun, 1998.

[2] G. W. Goerres, E. Kamel, T. N. Heidelberg *et al.*, "PET-CT image co-registration in the thorax: influence of respiration," *Eur J Nucl Med Mol Imaging,* vol. 29, no. 3, pp. 351-60, Mar, 2002.

[3] A. M. Alessio, and P. E. Kinahan, "Improved quantitation for PET/CT image reconstruction with system modeling and anatomical priors," *Med Phys,* vol. 33, no. 11, pp. 4095-103, Nov, 2006.

[4] M. Dawood, F. Büther, N. Lang *et al.*, "Respiratory gating in positron emission tomography: A quantitative comparison of different gating schemes," *Med Phys,* vol. 34, no. 7, pp. 3067-3076, 2007.

[5] J. Daouk, L. Fin, P. Bailly *et al.*, "Comparison of an original respiratory gated PET method, based on breath-hold CT, versus ungated PET," *Eur J Nucl Med,* vol. 34, no. Suppl 2, pp. S145, 2007.

[6] M. Defrise, P. E. Kinahan, D. W. Townsend *et al.*, "Exact and approximate rebinning algorithms for 3-D PET data," *IEEE Trans Med Imaging,* vol. 16, no. 2, pp. 145-58, Apr, 1997.

[7] P. E. Kinahan, D. W. Townsend, T. Beyer *et al.*, "Attenuation correction for a combined 3D PET/CT scanner," *Med Phys,* vol. 25, no. 10, pp. 2046-53, Oct, 1998.

[8] C. C. Watson, "New, faster, image-based scatter correction for 3D PET," *IEEE Transactions on Nuclear Science,* vol. 47, no. 4, pp. 1587-1594, aug, 2000.

[9] U. Nestle, S. Kremp, A. Schaefer-Schuler *et al.*, "Comparison of different methods for delineation of 18F-FDG PET-positive tissue for target volume definition in radiotherapy of patients with non-Small cell lung cancer," *J Nucl Med,* vol. 46, no. 8, pp. 1342-8, Aug, 2005.

[10] C. X. Wang, W. E. Snyder, G. Bilbro *et al.*, "Performance evaluation of filtered backprojection reconstruction and iterative reconstruction methods for PET images," *Comput Biol Med,* vol. 28, no. 1, pp. 13-24; discussion 24-5, Jan, 1998.

[11] L. Garnero, J. Fonroget, F. Coutand *et al.*, "Problèmes inverses en tomographie d'émission - Nouvelles tendances," *Imagerie, cohérence, information*, Annales de Physique 3, P. Chavel and P. Lalanne, eds., pp. 153-193, Paris: EDP sciences, 1999.